

# Comparative Analysis of RNA/Protein Dynamics for the Arginine-Rich-Binding Motif and Zinc-Finger-Binding Motif Proteins Encoded by HIV-1

Hui Wang,<sup>†</sup> Xiaojing Ma,<sup>†</sup> Yu-Shan Yeh,<sup>†</sup> Yongjin Zhu,<sup>†</sup> Matthew D. Daugherty,<sup>‡</sup> Alan D. Frankel,<sup>‡</sup> Karin Musier-Forsyth,<sup>§¶||††</sup> and Paul F. Barbara<sup>†\*</sup>

<sup>†</sup>Center for Nano and Molecular Science and Technology, Department of Chemistry and Biochemistry, University of Texas at Austin, Austin, Texas; <sup>‡</sup>Department of Biochemistry and Biophysics, University of California, San Francisco, California; and <sup>§</sup>Department of Chemistry, <sup>¶</sup>Department of Biochemistry, <sup>||</sup>Center for RNA Biology, and <sup>††</sup>Center for Retrovirus Research, Ohio State University, Columbus, Ohio

**ABSTRACT** We report a comparative study in which a single-molecule fluorescence resonance energy transfer approach was used to examine how the binding of two families of HIV-1 viral proteins to viral RNA hairpins locally changes the RNA secondary structures. The single-molecule fluorescence resonance energy transfer results indicate that the zinc finger protein (nucleocapsid) locally melts the TAR RNA and RRE-IIB RNA hairpins, whereas arginine-rich motif proteins (Tat and Rev) may strengthen the hairpin structures through specific binding interactions. Competition experiments show that Tat and Rev can effectively inhibit the nucleocapsid-chaperoned annealing of complementary DNA oligonucleotides to the TAR and RRE-IIB RNA hairpins, respectively. The competition binding data presented here suggest that the specific nucleic acid binding interactions of Tat and Rev can effectively compete with the general nucleic acid binding/chaperone functions of the nucleocapsid protein, and thus may in principle help regulate critical events during the HIV life cycle.

## INTRODUCTION

The advent of single-molecule fluorescence resonance energy transfer (SM-FRET), with its ability to unravel the complex structural dynamics of biomolecules (1–8), has made it possible to analyze RNA/protein dynamical interactions at the molecular level with unprecedented specificity, such as by obtaining direct information on the secondary structure of key functional ribonucleoprotein complexes (9–11). In this study we used SM-FRET in vitro to systematically compare and contrast the RNA/protein interactions for two critical RNA-binding motifs in HIV-1: the arginine-rich-binding motif (ARM) and the zinc-finger-binding motif. HIV-1 encodes two ARM regulatory proteins, Rev and Tat, and a zinc-finger-binding-motif protein, the multifunctional nucleocapsid (NC) protein. Our SM-FRET results regarding the interactions of Rev, Tat, and NC with a series of key viral RNA sequences give a clearer picture of how these two binding motifs differ in their sequence specificity, impact on RNA secondary structure, and chaperone-like nucleic acid annealing activity.

Rev functions through its oligomeric binding to the Rev response element (RRE), a 351-nucleotide-long sequence composed of complex stem-loop structures located in the *env* coding region of the viral genome (12–14). The IIB stem loop of RRE has been identified as the high-affinity Rev-binding site on RRE (15–17). The sequence and MFOLD (18) secondary structure of RRE IIB are shown in Fig. 1 and the proposed sites of Rev binding to IIB are

indicated by red arrows. As illustrated in Fig. 1, Rev harbors a nuclear localization signal (NLS) containing the ARM for RNA binding, the oligomerization domains for oligomeric protein assembly on RRE, and an activation domain for nuclear export (NES). Rev shuttles between the nucleus and the cytoplasm in vivo and binds the RRE region cooperatively to guide the export of unspliced and partially spliced genomic mRNA from the nucleus to the cytoplasm (13,17,19,20).

Tat functions as a highly efficient transcriptional activator of HIV-1 through binding to the *trans*-activating response (TAR) RNA hairpin (Fig. 1) located at the 5' end of the untranslated leader region of the viral mRNA (21–25). Tat is an 86-amino acid protein that contains a cysteine-rich domain, a core region composed of hydrophobic amino acids, a nuclear localization region containing the ARM (which is responsible for RNA recognition and binding), and a glutamine region. The proposed Tat-binding site on TAR RNA, the UCU bulge, is indicated by a red arrow in Fig. 1. The 20-amino-acid Tat peptide containing only the core region and the ARM (Fig. 1) has been reported to be sufficient for recognition and specific binding to TAR RNA (26,27), and was used in this study.

In contrast to Rev and Tat, NC can bind to various DNA and RNA hairpin structures (28). As shown in Fig. 1, HIV-1 NC is 55 amino acids long and has two nonequivalent CCHC-type zinc fingers, each of which strongly binds a zinc ion. NC is a multifunctional protein that plays a role in almost every step of the retroviral life cycle, from genomic packaging and assembly to reverse transcription and proviral DNA integration (28). Although some NC functions, such as genomic RNA packaging, are believed to involve sequence-specific binding to nucleic acids, NC also

Submitted July 20, 2010, and accepted for publication September 28, 2010.

\*Correspondence: p.barbara@mail.utexas.edu

Hui Wang's present address is Department of Chemistry and Biochemistry, University of South Carolina, Columbia, South Carolina.

Editor: Samuel Butcher.

© 2010 by the Biophysical Society  
0006-3495/10/11/3454/9 \$2.00

doi: 10.1016/j.bpj.2010.09.051



each band on the gels were quantified with the use of Quantity One software (Bio-Rad Laboratory, Hercules, CA). The binding curves were constructed by plotting the fraction of RNA bound with proteins,  $\theta$  (total bound RNA in all bands divided by the sum of bound and unbound RNAs) as a function of protein concentration. The apparent dissociation constants,  $K_d$ , for protein binding to RNAs can be obtained by fitting the data points with the Hill equation (17):

$$\theta = \frac{(P_0 - nR_0\theta)^n}{k_d^n + (P_0 - nR_0\theta)^n} \quad (1)$$

where  $R_0$  is the total concentration of RNA added in each lane (25 nM),  $P_0$  is the total concentration of proteins added in each lane, and  $n$  is the Hill coefficient that is related to the protein-binding stoichiometry. The  $K_d$  and  $n$ -values for each protein were obtained by curve-fitting to achieve the minimized difference between the experimentally measured and calculated  $\theta$ -values.

### Flow system for oligonucleotide annealing reactions

The annealing reactions were carried out in an in-house-built flow cell (30,33). Typically, the Cy5-labeled oligonucleotides, buffer solutions, and protein solutions were selectively flowed into the flow cell to react with the Cy3-labeled oligonucleotides immobilized on the coverslip surface. The details of the chamber assembly process and the immobilization of the oligonucleotides on the coverslip surface have been described elsewhere (30). All of the annealing reactions were carried out at room temperature in protein-binding buffer in an oxygen scavenger system (48) containing  $\beta$ -D(+)-glucose 3% w/v (Sigma-Aldrich, St. Louis, MO), glucose oxidase 0.1 mg/mL, and catalase 0.02 mg/mL (Roche Applied Science, Hague Road, IN). Then 2 mg/mL of Trolox (Fisher Scientific) or 1% v/v 2-mercaptoethanol (Fisher Scientific) were added to the mixtures to eliminate the blinking of molecules and generate longer-lasting single-molecule fluorescence signals (49). The protein-binding buffers were composed of 25 mM HEPES (pH 7.3), 40 mM NaCl, and 0.2 mM MgCl<sub>2</sub> (for TAR-related annealing experiments) or 1 mM MgCl<sub>2</sub> (for RRE IIB-related annealing experiments).

### Data collection and analysis

An in-house-built sample-scanning confocal optical/data collection system based on a Zeiss inverted microscope (33) was used in the SM-FRET experiments. The sample flow cell was scanned by a Queensgate X,Y scanning stage (NPW-XY-100A; Queensgate, Torquay, UK). A high numerical aperture, oil immersion microscope objective (Zeiss Fluor, 100 $\times$ , NA 1.3) was used for excitation (514 nm or 633 nm) and signal collection. The laser power focused on the samples was typically 8  $\mu$ W for Argon laser (514 nm) or 1  $\mu$ W for HeNe laser (633 nm). The donor fluorescence and acceptor fluorescence were separated by a dichroic beam splitter (Chroma 630 DCXR; Chroma Technology, Bellows Falls, VT) into two beams, and each was detected by an avalanche photodiode (APD, SPCM-AQR-15; Perkin-Elmer Optoelectronics, Vaudreuil, Canada). SM-FRET data were collected synchronously through separate detection channels for Cy3 and Cy5 fluorescence intensities.

The annealing reactions were initiated by flowing a freshly prepared protein solution plus Cy5-labeled oligonucleotides into the flowing sample cell. The scanning confocal fluorescence images were acquired several times during the course of the annealing reactions, and custom-written MATLAB programs (The MathWorks, Natick, MA) were used to find the molecules and calculate the FRET efficiency for each molecule. A unique advantage of this data collection mode is that photobleaching of Cy5 can be effectively eliminated (as verified by the 633 nm laser excited acceptor emission measurements) because each molecule is exposed to excitation lasers for very short periods of time ( $\sim$ 9 ms) during each scan, and we typically scan fewer than 10 images in total during each annealing experiment.

The corrected donor and acceptor intensities,  $I_D(t)$  and  $I_A(t)$ , respectively, were used to calculate the time trajectory of the apparent FRET efficiency,  $E_A(t)$ , according to:

$$E_A(t) = \frac{I_A(t)}{I_D(t) + I_A(t)} \quad (2)$$

$E_A(t)$  is related to the actual FRET efficiency,  $E_{\text{FRET}}(t)$ , by the inclusion of the dye quantum efficiencies,  $\phi_i$ , and detector quantum efficiencies,  $\eta_i$ , according to:

$$E_{\text{FRET}}(t) = \frac{I_A(t)}{I_A(t) + I_D(t) \frac{\phi_A \eta_A}{\phi_D \eta_D}} \quad (3)$$

In the case of the current experimental setup, it was determined that  $E_A(t) \approx E_{\text{FRET}}(t)$ . The collected donor and acceptor signals were corrected for background emission/noise and donor/acceptor crosstalk due to signal leakage as previously described (30,32).

## RESULTS AND DISCUSSION

### NC/Tat/TAR interactions

In this section we focus on a comparison of how NC and Tat, separately and in combination, interact with the TAR oligomers that are summarized in Table S1. We are especially concerned with how the presence of Tat inhibits the NC-chaperoned annealing reaction between TAR DNA and complementary TAR RNA or, alternatively, complementary cTAR DNA (30–34). The experiments included gel-mobility-shift assays to establish specific and nonspecific binding affinities for these nucleic acid binding proteins to a set of oligomers (see Fig. 2 for typical examples). These were followed by SM-FRET experiments on the rates and yields of the NC-chaperoned annealing reactions in the presence and absence of Tat.

Fig. 2 shows the results of gel-shift assays on Tat and NC binding to TAR sequences together with the binding isotherms obtained from the gel images. The apparent dissociation constants ( $K_d$ ) and Hill coefficients ( $n$ ) for the protein/nucleic-acid complexes determined by gel-shift assays are summarized in Table 1. It is worth mentioning that since the local environments of the gels are different from those in the flow cells for SM-FRET measurements, the  $K_d$ -values obtained from the gel-shift assays may not reflect the solution-binding affinities. Nevertheless, these values do provide valuable information for comparing the relative binding affinity and cooperativity of these viral proteins. In all cases, more than one copy of the protein can bind to the nucleic acid substrates at high protein concentrations, and the Hill coefficients are determined to be  $>1$ , indicating that the protein binding to the nucleic acid sequences is cooperative.

As shown in Fig. 2 A, Tat binds strongly to its target sequence on TAR RNA with a  $K_d$  of  $\sim$ 15 nM, but not to TAR DNA or the other non-TAR sequences (see Fig. S1), consistent with the ARM-binding motif assignment for this peptide (see Introduction). It is apparent from Fig. 2 A

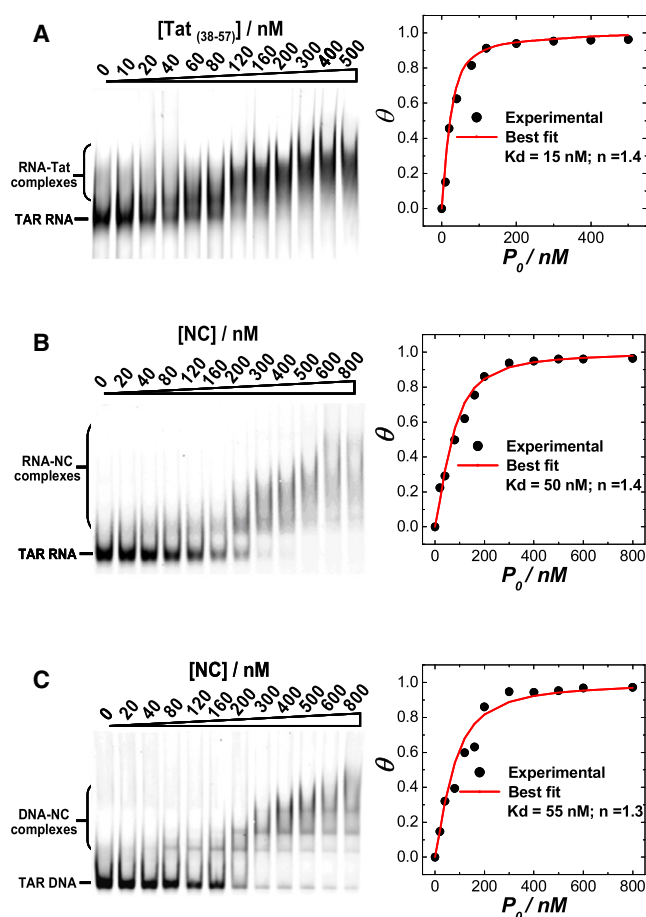


FIGURE 2 Electrophoresis gel-shift assay of (A) Tat binding to TAR RNA, (B) NC binding to TAR RNA, and (C) NC binding to TAR DNA. The left panels show the gel images, and the right panels show the corresponding binding isotherms with Hill equation curving-fitting.

that more than one copy of Tat can bind to one TAR RNA hairpin cooperatively ( $n = 1.4$ ) at high protein concentrations. In contrast to Tat, NC binds strongly to both TAR DNA and TAR RNA with  $K_d < 100$  nM (Fig. 2, B and C). NC is known to be able to bind to both single-stranded and double-stranded nucleic acids nonspecifically, with

**TABLE 1 Apparent dissociation constants ( $K_d$ ) and Hill coefficient ( $n$ ) for the protein/nucleic-acid complexes determined by gel-shift assays**

Protein	RNA or DNA		
	Tat	Rev	NC
TAR RNA	$K_d = 15 \pm 1$ nM $n = 1.4 \pm 0.1$	—	$K_d = 50 \pm 3$ nM $n = 1.4 \pm 0.1$
TAR DNA	—	—	$K_d = 55 \pm 6$ nM $n = 1.3 \pm 0.1$
cTAR DNA	—	—	$K_d = 120 \pm 9$ nM $n = 1.3 \pm 0.1$
RRE-IIB RNA	—	$K_d = 60 \pm 3$ nM $n = 1.5 \pm 0.1$	$K_d = 20 \pm 1$ nM $n = 1.8 \pm 0.1$

The dash indicates that no obvious protein binding was observed in protein concentrations ranging from 0 to 800 nM in these gel-shift assays.

a stronger binding preference for single-stranded regions (50–54). The  $K_d$ -values obtained from our gel-shift assays are in general agreement with the values reported in the literature (28). Binding affinity is highly dependent on solution ionic strength; however, binding affinities in the range of a few nanomolars to ~500 nM are typical for NC binding to nucleic acids under a variety of solution conditions.

The smearing of the bands for NC binding is consistent with previous reports that multiple copies of NC bind with a footprint of one NC per ~8 basepairs without strong sequence specificity to hairpin and fully duplexed DNA and RNA (43). It is important to note that although NC is known to melt structured DNA and RNA hairpins due to its binding preference for single-stranded nucleic acids, melting is not required for strong binding. Consistent with these trends, we observed strong binding ( $K_d \sim 200$  nM) to fully duplexed DNA (TAR-cTAR DNA duplex, in HEPES buffer), which should not be melted by NC (55). We also observed strong binding of NC to DNA and RNA with  $K_d < 100$  nM (see one example in Fig. 5 C) in the presence of ethylenediaminetetraacetic acid (EDTA), a chelating ligand that can be used to effectively extract the zinc ions from NC (56). EDTA is a strong zinc-binding agent with a  $K_d$  of  $\sim 10^{-16}$  M (57). In addition, EDTA binds zinc much more tightly than other common divalent metals, such as  $Mg^{2+}$  ( $K_d \sim 10^{-9}$  M) (57), which means that EDTA can selectively and effectively eject zinc from NC, especially under our experimental conditions where EDTA is at 0.5 mM and NC is at  $< 2$   $\mu$ M. In the absence of zinc, the zinc fingers can no longer maintain their properly folded structures that are crucial to the local melting of the duplex regions of the hairpin. However, the zincless NC does not show a significant decrease in its binding affinity to RNA substrates. These results are consistent with the notion that a non-sequence-specific electrostatic binding of NC to nucleic acids is an important, if not dominant, binding mode under these conditions. The basic residues of NC are probably responsible for the electrostatic interactions with the RNA substrates, and it is also possible that NC can fold into different conformations to accommodate productive electrostatic interactions even in the absence of  $Zn^{2+}$  binding (56,58).

It is interesting to examine whether the observed Tat and NC binding affinity pattern is reflected in how these proteins affect TAR annealing reactions. Typical SM-FRET data for the NC-induced annealing of immobilized TAR DNA with 5 nM TAR RNA and 800 nM NC in a flowing buffered solution are shown in Fig. S2. For the SM-FRET measurements, we used protein concentrations above the  $K_d$  to ensure saturating protein binding to the nucleic acid substrates. Each FRET trajectory  $E_A(t)$  in the upper panel corresponds to a single immobilized oligomer for which the apparent FRET value,  $E_A$ , switches from zero to unity when the annealing reaction occurs. A small portion of the molecules (typically 2–10%) show intermediate FRET

values (0.3–0.7), probably due to the presence of misfolded nucleic acids and/or long-lived reaction intermediates, or to dye-labeling issues. When single-molecule FRET trajectories exhibit a state with a FRET value near the boundaries of the range of 0–1, they may show transient excursions to FRET values  $< 0$  (when the acceptor intensity briefly dips into negative territory due to noise in the data) or  $> 1$  (when the donor signal goes into negative territory). The lower panel of Fig. S2 shows the fraction of annealed TAR DNA hairpins as a function of reaction time. The annealing percentage achieves a value  $> 50\%$  after  $\sim 45$  min, using a FRET threshold of 0.4 to distinguish the annealed and unannealed molecules. We previously described in detail how one can analyze such data to obtain accurate bimolecular annealing rate constants by assuming that the reactions are pseudo first-order (33,34).

The FRET histograms in Fig. 3, which were recorded for long periods of time (e.g., 1 h) after the reagents were mixed for an ensemble of hairpins, give a clear picture of the impact of Tat and NC on the annealing reaction. Under these conditions, the equilibrium mixture strongly favors the fully annealed duplexes. In the absence of either NC or Tat, the annealing is too slow to observe on this timescale and only the  $E_{\text{FRET}}(t) \sim 0$  peak in the histogram is present (Fig. 3 A). When the 800 nM NC is added to the TAR RNA/buffer solution, annealing becomes rapid enough to observe a significant  $E_{\text{FRET}} \sim 1$  peak in this time window (Fig. 3 B). The lack of 100% annealing is due primarily to unreactive, misfolded TAR RNA hairpins (33). In contrast to the chaperone-like activity of NC, Tat shows no evidence of catalyzing the annealing reaction (Fig. 3 C). Furthermore, Tat is observed to strongly inhibit the chaperone-like

activity of NC, as shown in Fig. 3 D. As previously shown (34), the corresponding DNA-only annealing reaction (i.e., TAR DNA + cTAR DNA) is also extremely slow without added NC, but becomes strongly catalyzed with NC present (Fig. 4, A and B), leading to a nearly 100% annealing yield within 1 h. For the TAR DNA + cTAR DNA case, Tat alone is unable to catalyze the annealing (Fig. 4 C), and adding Tat to the NC reaction has no measurable inhibitory effect (Fig. 4 D). This strongly suggests that Tat specifically binds to the TAR RNA hairpin, and that only through this specific binding is the inhibition of NC-chaperoned annealing accomplished.

The TAR DNA + TAR RNA annealing results can be rationalized by considering the previously proposed mechanism for NC chaperone activity (30). It has been hypothesized that NC partially melts both reactant hairpins, allowing for rapid nucleation of annealing initiated by base-pairing of short single-stranded regions. In previous studies we directly observed the melting process by investigating the SM-FRET of dual-labeled TAR hairpins with NC present (30,32). Furthermore, NC-induced partial melting was assigned to selective stabilization of melted secondary structures of TAR DNA and TAR RNA by NC binding, resulting from NC's binding preference for single-stranded regions. It has been proposed that the nucleation of annealing occurs right at the locally melted regions in an encounter complex that is comprised of partially melted TAR DNA and TAR RNA or cTAR DNA hairpins associated with multiple copies of NC proteins (31,34). The NC-chaperoned annealing is schematically shown in Scheme S1. The inhibitory mechanism of Tat on TAR DNA + TAR RNA annealing may simply be due to Tat's ability to block the binding

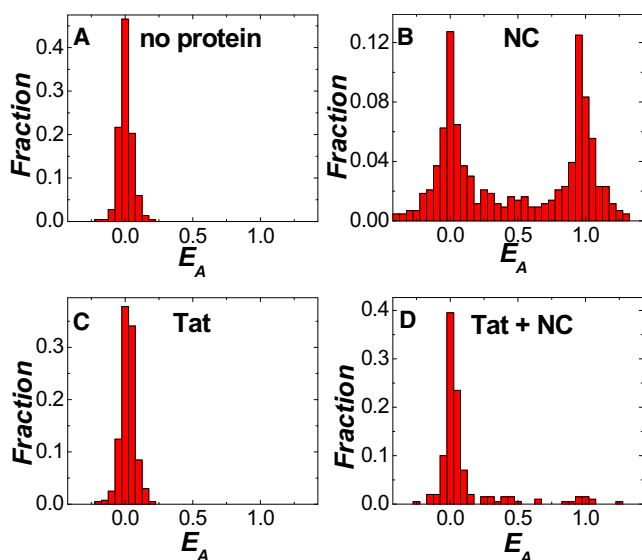


FIGURE 3 FRET histograms obtained from SM-FRET measurements after flowing in 5 nM Cy5-labeled TAR RNA over immobilized Cy3-labeled TAR DNA for 1 h in the presence of (A) no proteins, (B) 800 nM NC, (C) 500 nM Tat<sub>(38-57)</sub>, and (D) 500 nM Tat<sub>(38-57)</sub> and 800 nM NC.

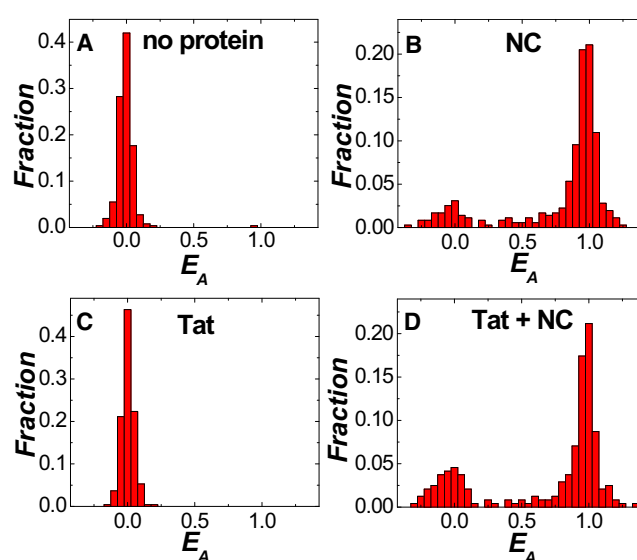


FIGURE 4 FRET histograms obtained from SM-FRET measurements after flowing in 5 nM Cy5-labeled cTAR DNA over immobilized Cy3-labeled TAR DNA for 45 min in the presence of (A) no proteins, (B) 800 nM NC, (C) 500 nM Tat<sub>(38-57)</sub>, and (D) 500 nM Tat<sub>(38-57)</sub> and 800 nM NC.

of NC to TAR RNA, thus suppressing NC-induced melting of TAR RNA.

The hypothesis that Tat binding to TAR RNA effectively suppresses partial melting is consistent with the evidence that Tat binds to a secondary structure with basepairs intact that are adjacent to the red bases in Fig. 1 for TAR RNA. Tat's preference for nonmelted secondary structures of TAR RNA is also probably a factor in its lack of chaperone activity for TAR RNA + TAR DNA annealing. Since Tat only binds strongly to TAR RNA, not to cTAR DNA (Table 1), it is not surprising that Tat has no inhibitory effect on NC-chaperoned TAR DNA + cTAR DNA annealing, as shown in Fig. 4 D. Finally, as a negative control, we also investigated the effect of added Rev on the TAR RNA + TAR DNA annealing reaction (Fig. S3). The absence of an inhibitory effect for Rev on NC's chaperone activity for this annealing reaction is as expected, considering the lack of significant binding of Rev to these hairpins (Table 1).

### NC/Rev/RRE interactions

In this section, we generalize our comparative understanding of ARM versus zinc-finger binding proteins obtained by examining the binding and NC-chaperoned annealing for a different ARM protein and target RNA sequence combination, namely, Rev and the RRE-IIB RNA. In analogy to Tat binding to TAR RNA, the ARM protein Rev binds specifically to its target sequence RRE IIB (Fig. 5 A), but does not bind to either TAR RNA or TAR DNA (Table 1). Multiple copies of NC are observed to bind cooperatively to RRE IIB (Fig. 5 B and Table 1), due to the strong nonsequence-specific nucleic acid binding propensity of NC described above. To examine the role of zinc in the binding of NC, we added 0.5 mM EDTA to the NC-binding buffer to extract the zinc ions out of the zinc fingers of NC. The gel was also run in 0.5× Tris-Borate-EDTA buffer instead of 0.5× Tris-Borate buffer to ensure the presence of EDTA throughout the whole process. The results (Fig. 5 C) clearly show that zincless NC can still bind RRE-IIB without a significant decrease in binding affinity. However, instead of multiple discrete bands corresponding to IIB-NC nucleoprotein complexes with varying binding stoichiometries, only one discrete band was observed on the gel in addition to the free RNA band.

To explore the generality of NC's chaperone-like activity and directly compare Rev/NC/RRE interactions, we designed two annealing assays in which a complementary DNA oligomer (cIIB-1 DNA or cIIB-2 DNA; see Table S2) is annealed to RRE IIB RNA. In the absence of NC, both RRE IIB annealing assays exhibit FRET histograms (Fig. 6, A and E) with an  $E_A \sim 0$  peak only, consistent with immeasurably slow annealing under these conditions. When NC is added, the FRET histograms for both annealing reactions exhibit a measurable  $E_A \sim 0.9$  peak, consistent with NC-induced annealing (Fig. 6, B and F). Presumably, NC

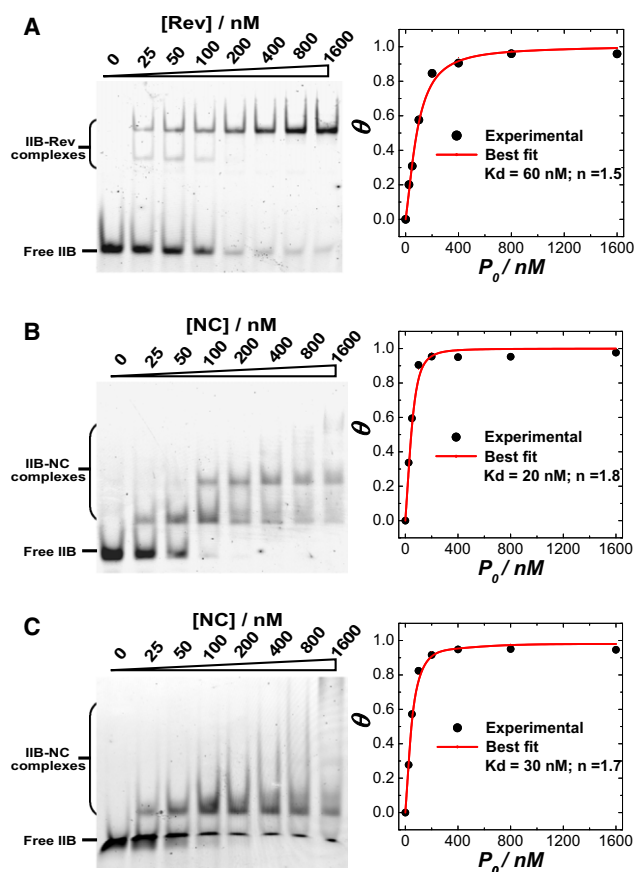


FIGURE 5 Electrophoresis gel-shift assays of (A) Rev, (B) NC, and (C) zincless NC binding to RRE-IIB RNA. The left panels show the gel images, and the right panels show the corresponding binding isotherms with Hill equation curving-fitting.

binding to RRE-IIB RNA locally melts the duplexed regions in the hairpin secondary structure (as predicted by MFOLD), allowing for the nucleation of basepairing between RRE IIB and the complementary DNA oligonucleotides. In the case of RRE IIB + cIIB-1 DNA annealing, NC may also accelerate annealing by melting the basepairing of cIIB-1 DNA. However, we did not explore this aspect of the reaction further. To verify that the zinc fingers of NC are also crucial for NC's chaperone activity in IIB annealing reactions, we examined the single-molecule annealing assays in the presence of EDTA. As expected, EDTA completely suppresses the  $E_A \sim 0.9$  peak (Fig. S4), indicating that the zinc fingers are crucial for NC's chaperone activity. To confirm that melting of duplexed bases is the reason for annealing in the two RRE IIB annealing assays, we investigated an annealing reaction between fully complementary RNA and DNA sequences (Half-IIB RNA + cIIB-2 DNA) that should have no significant intramolecular basepairing as predicted by MFOLD (18). Fig. S5 shows that Half-IIB RNA + cIIB-2 DNA annealing exhibits a measurable  $E_A \sim 1$  peak even in the absence of NC. In contrast to annealing between hairpins, the annealing between these two linear single-stranded

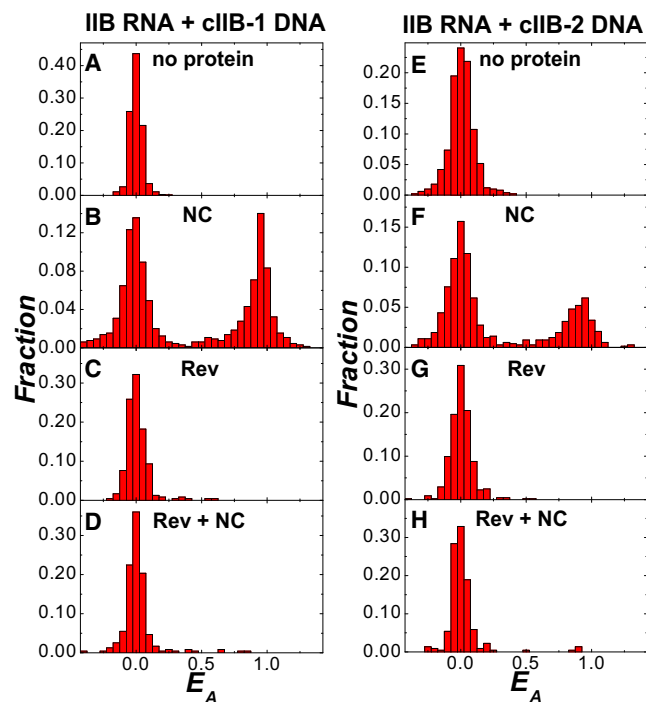


FIGURE 6 (Left column) FRET histograms obtained from SM-FRET measurements after flowing in 30 nM cIIB-1 DNA over immobilized IIB for 1 h in the presence of (A) no proteins, (B) 800 nM NC, (C) 800 nM Rev, and (D) 800 nM Rev and 800 nM NC. (Right column) FRET histograms obtained after flowing in 80 nM cIIB-2 DNA over immobilized IIB for 2 h in the presence of (E) no proteins, (F) 800 nM NC, (G) 800 nM Rev, and (H) 800 nM Rev and 800 nM NC.

sequences shows relatively fast kinetics even in the absence of the protein chaperone because it does not require the melting of duplexed regions of hairpins.

We used RRE IIB annealing assays to directly test whether Rev has chaperone activity similar to that of NC. As shown in Fig. 6, C and G, no annealing is observed between RRE-IIB and either cIIB-1 DNA or cIIB-2 DNA in the presence of 800 nM Rev, indicating a lack of chaperone activity for Rev. In addition, the NC-induced annealing of cIIB-1 DNA and cIIB-2 DNA to RRE IIB is completely inhibited in the presence of 800 nM Rev, as is clearly shown in Fig. 6, D and H. We hypothesize that Rev binding to TAR RNA effectively suppresses partial melting of the IIB RNA hairpin, which is crucial for the annealing reactions. Such inhibitory effects on NC-chaperoned annealing are believed to arise from two main consequences of Rev binding. First, Rev may block the binding of multiple copies of NC to the bulge regions of RRE IIB RNA, thus suppressing NC-induced melting of IIB RNA. Second, Rev may also strengthen the RRE IIB hairpin structures by creating additional contacts between the bases in the bulge regions. Previous biochemical and structural studies (15,59,60) showed that recognition of stem-loop IIB of the RRE by Rev requires a purine-rich bubble that contains two purine-purine basepairs separated

by a bulged uridine base, which helps widen the RNA major groove and allows deep penetration of the arginine-rich  $\alpha$ -helix of Rev. Structural analysis revealed that binding of Rev to IIB RNA induces the formation of the purine base-pairs G12-A33 and G13-G31, suggesting a decrease in hairpin flexibility upon Rev binding.

## CONCLUSIONS

Using a SM-FRET approach, we performed a comparative study on how the binding of two families of HIV-1 viral proteins to viral RNA hairpins locally changes the secondary structures of the RNAs. Our SM-FRET results indicate that the zinc-finger protein (NC) locally melts the RRE-IIB and TAR RNA hairpins, whereas the ARM proteins (Rev and Tat) may strengthen the hairpin structures through specific binding interactions. Competition experiments (as summarized in Table S3) show that the presence of Rev and Tat can effectively inhibit the NC-binding-induced local melting of RRE-IIB and TAR RNA hairpins, respectively. The data suggest that in HIV-1, the arginine-rich motifs of Rev and Tat may help stabilize the RNA hairpin structures, which likely inhibits the local melting of the hairpins induced by NC.

Previous studies have suggested that HIV-1 Tat can promote nucleic acid restructuring reactions, including tRNA primer annealing onto the primer binding site (61), as well as complementary TAR DNA hairpin annealing (62,63). In contrast to those studies, we see no evidence of nucleic acid chaperone activity by Tat<sub>38-57</sub> using the RNA/DNA oligonucleotides investigated here. It is known that tRNA primer annealing does not require the zinc-finger structures of NC and can be facilitated by polyLys (64). Thus, it is not too surprising that Tat, which contains a basic ARM, can also facilitate tRNA primer annealing (61). However, for annealing between TAR hairpins, local melting of the hairpin structures is necessary to catalyze the annealing reactions. Tat (both the full-length protein and the peptide containing the basic domain) is unable to melt the duplexed regions of TAR sequences (63), although it may promote TAR/cTAR annealing, presumably through some other motions involving nonspecific attraction between the peptide-bound oligonucleotides (62,63). In contrast to Tat, NC's chaperone activity arises from two main consequences of protein binding: 1), partial melting of the duplex regions of nucleic acid hairpins; and 2), screening of the negative charges of the hairpins, which facilitates the formation of the encounter complexes.

It is known that NC is a general nucleic acid chaperone that can catalyze many nucleic acid rearrangements throughout the HIV life cycle, whereas Tat and Rev function via specific nucleic acid binding interactions in the nucleus. Previous subcellular fractionation studies of HIV-1-infected cells showed that NC was present only in the cytoplasm 1 h postinfection, but had partly migrated to the nucleus after

8 h (65). Roles for NC in stimulating viral DNA integration (66–68) and HIV-1 early mRNA expression (69,70) have also been proposed. The competition binding data presented here suggest that the specific nucleic acid binding interactions of Tat and Rev can effectively compete with NC, and thus can in principle regulate critical events in the HIV life cycle despite the presence of a robust nucleic acid binding/chaperone protein such as NC.

## SUPPORTING MATERIAL

Three tables, one scheme, and five figures are available at [http://www.biophysj.org/biophysj/supplemental/S0006-3495\(10\)01201-4](http://www.biophysj.org/biophysj/supplemental/S0006-3495(10)01201-4).

This work was supported by grants from the National Institutes of Health (GM065056 to K.M.-F. and P50 GM082250 to A.D.F.) and the Welch Foundation (to P.F.B.).

## REFERENCES

- Zhuang, X. W., H. Kim, ..., S. Chu. 2002. Correlating structural dynamics and function in single ribozyme molecules. *Science*. 296:1473–1476.
- Myong, S., I. Rasnik, ..., T. Ha. 2005. Repetitive shuttling of a motor protein on DNA. *Nature*. 437:1321–1325.
- Weiss, S. 2000. Measuring conformational dynamics of biomolecules by single molecule fluorescence spectroscopy. *Nat. Struct. Biol.* 7:724–729.
- Schuler, B., E. A. Lipman, and W. A. Eaton. 2002. Probing the free-energy surface for protein folding with single-molecule fluorescence spectroscopy. *Nature*. 419:743–747.
- Lu, H. P., L. M. Iakoucheva, and E. J. Ackerman. 2001. Single-molecule conformational dynamics of fluctuating noncovalent DNA-protein interactions in DNA damage recognition. *J. Am. Chem. Soc.* 123:9184–9185.
- Lu, Q., H. P. Lu, and J. Wang. 2007. Exploring the mechanism of flexible biomolecular recognition with single molecule dynamics. *Phys. Rev. Lett.* 98:128105.
- Rueda, D., G. Bokinsky, ..., N. G. Walter. 2004. Single-molecule enzymology of RNA: essential functional groups impact catalysis from a distance. *Proc. Natl. Acad. Sci. USA*. 101:10066–10071.
- Liu, R. C., D. H. Hu, ..., H. P. Lu. 2006. Revealing two-state protein-protein interactions of calmodulin by single-molecule spectroscopy. *J. Am. Chem. Soc.* 128:10034–10042.
- Munro, J. B., R. B. Altman, ..., S. C. Blanchard. 2007. Identification of two distinct hybrid state intermediates on the ribosome. *Mol. Cell*. 25:505–517.
- Fei, J., P. Kosuri, ..., R. L. Gonzalez, Jr. 2008. Coupling of ribosomal L1 stalk and tRNA dynamics during translation elongation. *Mol. Cell*. 30:348–359.
- Theissen, B., A. R. Karow, ..., D. Klostermeier. 2008. Cooperative binding of ATP and RNA induces a closed conformation in a DEAD box RNA helicase. *Proc. Natl. Acad. Sci. USA*. 105:548–553.
- Frankel, A. D., and J. A. T. Young. 1998. HIV-1: fifteen proteins and an RNA. *Annu. Rev. Biochem.* 67:1–25.
- Pollard, V. W., and M. H. Malim. 1998. The HIV-1 Rev protein. *Annu. Rev. Microbiol.* 52:491–532.
- Pond, S. J. K., W. K. Ridgeway, ..., D. P. Millar. 2009. HIV-1 Rev protein assembles on viral RNA one molecule at a time. *Proc. Natl. Acad. Sci. USA*. 106:1404–1408.
- Battiste, J. L., H. Y. Mao, ..., J. R. Williamson. 1996.  $\alpha$ -Helix-RNA major groove recognition in an HIV-1 rev peptide-RRE RNA complex. *Science*. 273:1547–1551.
- Tiley, L. S., M. H. Malim, ..., B. R. Cullen. 1992. Identification of a high-affinity RNA-binding site for the human immunodeficiency virus type 1 Rev protein. *Proc. Natl. Acad. Sci. USA*. 89:758–762.
- Daugherty, M. D., I. D’Orso, and A. D. Frankel. 2008. A solution to limited genomic capacity: using adaptable binding surfaces to assemble the functional HIV Rev oligomer on RNA. *Mol. Cell*. 31:824–834.
- Zuker, M. 2003. Mfold web server for nucleic acid folding and hybridization prediction. *Nucleic Acids Res.* 31:3406–3415.
- Malim, M. H., J. Hauber, ..., B. R. Cullen. 1989. The HIV-1 rev transactivator acts through a structured target sequence to activate nuclear export of unspliced viral mRNA. *Nature*. 338:254–257.
- Hope, T. J. 1999. The ins and outs of HIV Rev. *Arch. Biochem. Biophys.* 365:186–191.
- Feng, S., and E. C. Holland. 1988. HIV-1 tat trans-activation requires the loop sequence within tar. *Nature*. 334:165–167.
- Weeks, K. M., C. Ampe, ..., D. M. Crothers. 1990. Fragments of the HIV-1 Tat protein specifically bind TAR RNA. *Science*. 249:1281–1285.
- Cordingley, M. G., R. L. LaFemina, ..., R. J. Colonno. 1990. Sequence-specific interaction of Tat protein and Tat peptides with the transactivation-responsive sequence element of human immunodeficiency virus type 1 in vitro. *Proc. Natl. Acad. Sci. USA*. 87:8985–8989.
- Frankel, A. D. 1992. Peptide models of the Tat-TAR protein-RNA interaction. *Protein Sci.* 1:1539–1542.
- Calnan, B. J., B. Tidor, ..., A. D. Frankel. 1991. Arginine-mediated RNA recognition: the arginine fork. *Science*. 252:1167–1171.
- Derse, D., M. Carvalho, ..., B. M. Peterlin. 1991. A minimal lentivirus Tat. *J. Virol.* 65:7012–7015.
- Tan, R. Y., A. Brodsky, ..., A. D. Frankel. 1997. RNA recognition by HIV-1 Tat and Rev. *Semin. Virol.* 8:186–193.
- Levin, J. G., J. H. Guo, ..., K. Musier-Forsyth. 2005. Nucleic acid chaperone activity of HIV-1 nucleocapsid protein: critical role in reverse transcription and molecular mechanism. *Prog. Nucleic Acid Res. Mol. Biol.* 80:217–286.
- Guo, J. H., T. Y. Wu, ..., J. G. Levin. 2000. Zinc finger structures in the human immunodeficiency virus type 1 nucleocapsid protein facilitate efficient minus- and plus-strand transfer. *J. Virol.* 74:8980–8988.
- Cosa, G., E. J. Harbron, ..., P. F. Barbara. 2004. Secondary structure and secondary structure dynamics of DNA hairpins complexed with HIV-1 NC protein. *Biophys. J.* 87:2759–2767.
- Liu, H. W., G. Cosa, ..., P. F. Barbara. 2005. Single-molecule FRET studies of important intermediates in the nucleocapsid-protein-chaperoned minus-strand transfer step in HIV-1 reverse transcription. *Biophys. J.* 89:3470–3479.
- Cosa, G., Y. N. Zeng, ..., P. F. Barbara. 2006. Evidence for non-two-state kinetics in the nucleocapsid protein chaperoned opening of DNA hairpins. *J. Phys. Chem. B*. 110:2419–2426.
- Liu, H. W., Y. N. Zeng, ..., P. F. Barbara. 2007. Insights on the role of nucleic acid/protein interactions in chaperoned nucleic acid rearrangements of HIV-1 reverse transcription. *Proc. Natl. Acad. Sci. USA*. 104:5261–5267.
- Zeng, Y. N., H. W. Liu, ..., P. F. Barbara. 2007. Probing nucleation, reverse annealing, and chaperone function along the reaction path of HIV-1 single-strand transfer. *Proc. Natl. Acad. Sci. USA*. 104:12651–12656.
- Vo, M. N., G. Barany, ..., K. Musier-Forsyth. 2009. HIV-1 nucleocapsid protein switches the pathway of transactivation response element RNA/DNA annealing from loop-loop “kissing” to “zipper”. *J. Mol. Biol.* 386:789–801.
- Vo, M. N., G. Barany, ..., K. Musier-Forsyth. 2006. Mechanistic studies of mini-TAR RNA/DNA annealing in the absence and presence of HIV-1 nucleocapsid protein. *J. Mol. Biol.* 363:244–261.
- Hong, M. K., E. J. Harbron, ..., K. Musier-Forsyth. 2003. Nucleic acid conformational changes essential for HIV-1 nucleocapsid protein-

- mediated inhibition of self-priming in minus-strand transfer. *J. Mol. Biol.* 325:1–10.
38. You, J. C., and C. S. McHenry. 1994. Human immunodeficiency virus nucleocapsid protein accelerates strand transfer of the terminally redundant sequences involved in reverse transcription. *J. Biol. Chem.* 269:31491–31495.
  39. Darlix, J. L., M. Lapadat-Tapolsky, ..., B. P. Roques. 1995. First glimpses at structure-function relationships of the nucleocapsid protein of retroviruses. *J. Mol. Biol.* 254:523–537.
  40. Rein, A., L. E. Henderson, and J. G. Levin. 1998. Nucleic-acid-chaperone activity of retroviral nucleocapsid proteins: significance for viral replication. *Trends Biochem. Sci.* 23:297–301.
  41. Bernacchi, S., S. Stoylov, ..., Y. Mély. 2002. HIV-1 nucleocapsid protein activates transient melting of least stable parts of the secondary structure of TAR and its complementary sequence. *J. Mol. Biol.* 317:385–399.
  42. Azoulay, J., J. P. Clamme, ..., Y. Mély. 2003. Destabilization of the HIV-1 complementary sequence of TAR by the nucleocapsid protein through activation of conformational fluctuations. *J. Mol. Biol.* 326:691–700.
  43. Lapadat-Tapolsky, M., H. De Rocquigny, ..., J. L. Darlix. 1993. Interactions between HIV-1 nucleocapsid protein and viral DNA may have important functions in the viral life cycle. *Nucleic Acids Res.* 21:831–839.
  44. Dib-Hajj, F., R. Khan, and D. P. Giedroc. 1993. Retroviral nucleocapsid proteins possess potent nucleic acid strand renaturation activity. *Protein Sci.* 2:231–243.
  45. Stoylov, S. P., C. Vuilleumier, ..., Y. Mély. 1997. Ordered aggregation of ribonucleic acids by the human immunodeficiency virus type 1 nucleocapsid protein. *Biopolymers.* 41:301–312.
  46. Le Cam, E., D. Coulaud, ..., Y. Mély. 1998. Properties and growth mechanism of the ordered aggregation of a model RNA by the HIV-1 nucleocapsid protein: an electron microscopy investigation. *Biopolymers.* 45:217–229.
  47. Landes, C. F., Y. N. Zeng, ..., P. F. Barbara. 2007. Single-molecule study of the inhibition of HIV-1 transactivation response region DNA/DNA annealing by argininamide. *J. Am. Chem. Soc.* 129:10181–10188.
  48. Ha, T. 2001. Single-molecule fluorescence methods for the study of nucleic acids. *Curr. Opin. Struct. Biol.* 11:287–292.
  49. Rasnik, I., S. A. McKinney, and T. Ha. 2006. Nonblinking and long-lasting single-molecule fluorescence imaging. *Nat. Methods.* 3:891–893.
  50. Berkowitz, R., J. Fisher, and S. P. Goff. 1996. RNA packaging. *Curr. Top. Microbiol. Immunol.* 214:177–218.
  51. Wu, J. Q., A. Ozarowski, ..., J. R. Casas-Finet. 1997. Binding of the nucleocapsid protein of type 1 human immunodeficiency virus to nucleic acids studied using phosphorescence and optically detected magnetic resonance. *Biochemistry.* 36:12506–12518.
  52. Urbaneja, M. A., M. Wu, ..., R. L. Karpel. 2002. HIV-1 nucleocapsid protein as a nucleic acid chaperone: spectroscopic study of its helix-destabilizing properties, structural binding specificity, and annealing activity. *J. Mol. Biol.* 318:749–764.
  53. Fisher, R. J., A. Rein, ..., L. E. Henderson. 1998. Sequence-specific binding of human immunodeficiency virus type 1 nucleocapsid protein to short oligonucleotides. *J. Virol.* 72:1902–1909.
  54. Vuilleumier, C., E. Bombarda, ..., Y. Mély. 1999. Nucleic acid sequence discrimination by the HIV-1 nucleocapsid protein NCp7: a fluorescence study. *Biochemistry.* 38:16816–16825.
  55. Wang, H., Y. S. Yeh, and P. F. Barbara. 2009. HIV-1 nucleocapsid protein bends double-stranded nucleic acids. *J. Am. Chem. Soc.* 131:15534–15543.
  56. Cruceanu, M., M. A. Urbaneja, ..., M. C. Williams. 2006. Nucleic acid binding and chaperone properties of HIV-1 Gag and nucleocapsid proteins. *Nucleic Acids Res.* 34:593–605.
  57. Nyborg, J. K., and O. B. Peersen. 2004. That zincing feeling: the effects of EDTA on the behaviour of zinc-binding transcriptional regulators. *Biochem. J.* 381:e3–e4.
  58. Urbaneja, M. A., B. P. Kane, ..., J. R. Casas-Finet. 1999. Binding properties of the human immunodeficiency virus type 1 nucleocapsid protein p7 to a model RNA: elucidation of the structural determinants for function. *J. Mol. Biol.* 287:59–75.
  59. Ye, X. M., A. Gorin, ..., D. J. Patel. 1996. Deep penetration of an  $\alpha$ -helix into a widened RNA major groove in the HIV-1 rev peptide-RNA aptamer complex. *Nat. Struct. Biol.* 3:1026–1033.
  60. Battiste, J. L., R. Y. Tan, ..., J. R. Williamson. 1994. Binding of an HIV Rev peptide to Rev responsive element RNA induces formation of purine-purine base pairs. *Biochemistry.* 33:2741–2747.
  61. Kameoka, M., M. Morgan, ..., M. A. Wainberg. 2002. The Tat protein of human immunodeficiency virus type 1 (HIV-1) can promote placement of tRNA primer onto viral RNA and suppress later DNA polymerization in HIV-1 reverse transcription. *J. Virol.* 76:3637–3645.
  62. Kuciak, M., C. Gabus, ..., J. L. Darlix. 2008. The HIV-1 transcriptional activator Tat has potent nucleic acid chaperoning activities in vitro. *Nucleic Acids Res.* 36:3389–3400.
  63. Boudier, C., R. Storck, ..., Y. Mély. 2010. The mechanism of HIV-1 Tat-directed nucleic acid annealing supports its role in reverse transcription. *J. Mol. Biol.* 400:487–501.
  64. Hargittai, M. R. S., A. T. Mangla, ..., K. Musier-Forsyth. 2001. HIV-1 nucleocapsid protein zinc finger structures induce tRNA(Lys,3) structural changes but are not critical for primer/template annealing. *J. Mol. Biol.* 312:985–997.
  65. Gallay, P., T. Hope, ..., D. Trono. 1997. HIV-1 infection of nondividing cells through the recognition of integrase by the importin/karyopherin pathway. *Proc. Natl. Acad. Sci. USA.* 94:9825–9830.
  66. Carteau, S., R. J. Gorelick, and F. D. Bushman. 1999. Coupled integration of human immunodeficiency virus type 1 cDNA ends by purified integrase in vitro: stimulation by the viral nucleocapsid protein. *J. Virol.* 73:6670–6679.
  67. Gao, K., R. J. Gorelick, ..., F. Bushman. 2003. Cofactors for human immunodeficiency virus type 1 cDNA integration in vitro. *J. Virol.* 77:1598–1603.
  68. Thomas, J. A., T. D. Gagliardi, ..., R. J. Gorelick. 2006. Human immunodeficiency virus type 1 nucleocapsid zinc-finger mutations cause defects in reverse transcription and integration. *Virology.* 353:41–51.
  69. Zhang, J. L., and C. S. Crumpacker. 2002. Human immunodeficiency virus type 1 nucleocapsid protein nuclear localization mediates early viral mRNA expression. *J. Virol.* 76:10444–10454.
  70. Zhang, J. L., P. L. Sharma, and C. S. Crumpacker. 2000. Enhancement of the basal-level activity of HIV-1 long terminal repeat by HIV-1 nucleocapsid protein. *Virology.* 268:251–263.

## Supplementary Information

### **A comparative analysis of RNA/protein dynamics for the arginine-rich-binding motif and zinc-finger-binding motif proteins encoded by HIV-1**

Hui Wang <sup>\*,¶</sup>, Xiaojing Ma <sup>\*</sup>, Yu-Shan Yeh <sup>\*</sup>, Yongjin Zhu <sup>\*</sup>, Matthew D. Daugherty <sup>†</sup>, Alan D. Frankel <sup>†</sup>, Karin Musier-Forsyth <sup>‡</sup>, and Paul F. Barbara <sup>\*,§</sup>

*\* Center for Nano and Molecular Science and Technology, Department of Chemistry and Biochemistry, The University of Texas at Austin, Austin, TX 78712*

*† Department of Biochemistry and Biophysics, University of California, San Francisco, CA 94143*

*‡ Departments of Chemistry and Biochemistry, Center for RNA Biology, and Center for Retrovirus Research, The Ohio State University, Columbus, OH 43210*

*§ To whom correspondence should be addressed. Email: [p.barbara@mail.utexas.edu](mailto:p.barbara@mail.utexas.edu)*

*¶ Current address: Department of Chemistry and Biochemistry, The University of South Carolina, Columbia, SC 29208. Email: [wang.hui@chem.sc.edu](mailto:wang.hui@chem.sc.edu)*

## Synthesis of HIV-1 Rev protein and Tat<sub>(38-57)</sub> peptide

The HIV-1 Rev protein utilized in these studies contains only a single cysteine, which is appended to the C-terminus of the 116 amino acid Rev protein. Using standard site-directed mutagenesis protocols (Stratagene), the previously described pHGB1-Rev construct (1) was modified to contain serines in the place of naturally occurring cysteines (C85S/C89S) and a unique cysteine (C117). The protein was prepared by *E. coli* expression and Ni-NTA purification as described previously with the following modifications (1). Following lysis, RNase A (50 µg/ml) and RNase T1 (50 U/ml) (Roche) were added as well as NaCl to 2M. Immediately following elution from the Ni-NTA resin (Qiagen), yeast tRNA (Invitrogen) was added to stoichiometric amounts with purified HG-Rev protein. Dialysis, TEV proteolysis and subsequent purification were as previously described (1). Purified protein was quantified by SDS-PAGE and immediately aliquoted and frozen in liquid nitrogen.

The Tat<sub>(38-57)</sub> peptide was synthesized using Rink amide resin on a Applied Biosystems Model 433A peptide synthesizer and standard Fmoc chemistry. The peptide was cleaved from the resin, deprotected and purified by HPLC on a C4 reverse-phase column using an acetonitrile gradient in 0.1% trifluoroacetic acid (TFA).

---

(1) Daugherty, M. D., I. D'Orso, and A. D. Frankel. 2008. A solution to limited genomic capacity: Using adaptable binding surfaces to assemble the functional HIV Rev oligomer on RNA. *Mol. Cell* 31:824-834.

## Detailed experimental conditions for gel-shift assays:

The gel-shift assays for Tat-binding were performed by incubating oligonucleotides with Tat<sub>(38-57)</sub> peptide at room temperature in 20 µl of binding mixtures containing 20 mM Tris base (pH7.5), 100 mM NaCl, 10 mM DTT, 0.1% Triton-100, 0.2 mM Mg<sup>2+</sup>, and 10% glycerol. The gel-running buffer was 0.5X TBE (Tris-Borate-EDTA).

The gel-shift assay for Rev-binding were performed by incubating oligonucleotides with Rev at 4°C in 20 µl of binding mixtures containing 10 mM HEPES (pH = 7.3), 100 mM NaCl, 1 mM DTT, 0.5 mM EDTA, 1 mM MgCl<sub>2</sub>, and 10% glycerol. The gel-running buffer was 0.5X TBE.

The gel-shift assays for NC-binding were performed by incubating oligonucleotides with NC at room temperature in 20 µl of binding mixtures containing 25 mM HEPES (pH = 7.3), 40 mM NaCl, 0.2 mM MgCl<sub>2</sub>, and 10 % glycerol. The gel-running buffer was 0.5X TB (Tris-Borate).

10X TBE buffer: 890 mM Tris-base, 890 mM Boric Acid, 20 mM EDTA (disodium).

10X TB buffer: 890 mM Tris-base, 890 mM Boric Acid.

**Table S1.** Primary sequences of TAR-related oligonucleotides and schematics illustrating the annealing reactions.

Oligonucleotides	Primary sequences
TAR DNA	5'- Cy3-TGGGTTCCCTAGTTAGCCAGAGA GCTCT(biotin)CAGGCAGATCTGGTCTAA CCAGAGAGACCCTTT -3'
TAR RNA	5'- GGGUCUCUCUGGUUAGACCAGAUCU GAGCCUGAGAGCUCUCUGGCUAACUAG GGAACCCUUUU-Cy5 -3'
cTAR DNA	5'-TTTTGGGTCTCTCTGGTTAGACCAG ATCTGAGCCTGAGAGCTCTCTGGCTAA CTAGGGAACCCT-Cy5 -3'

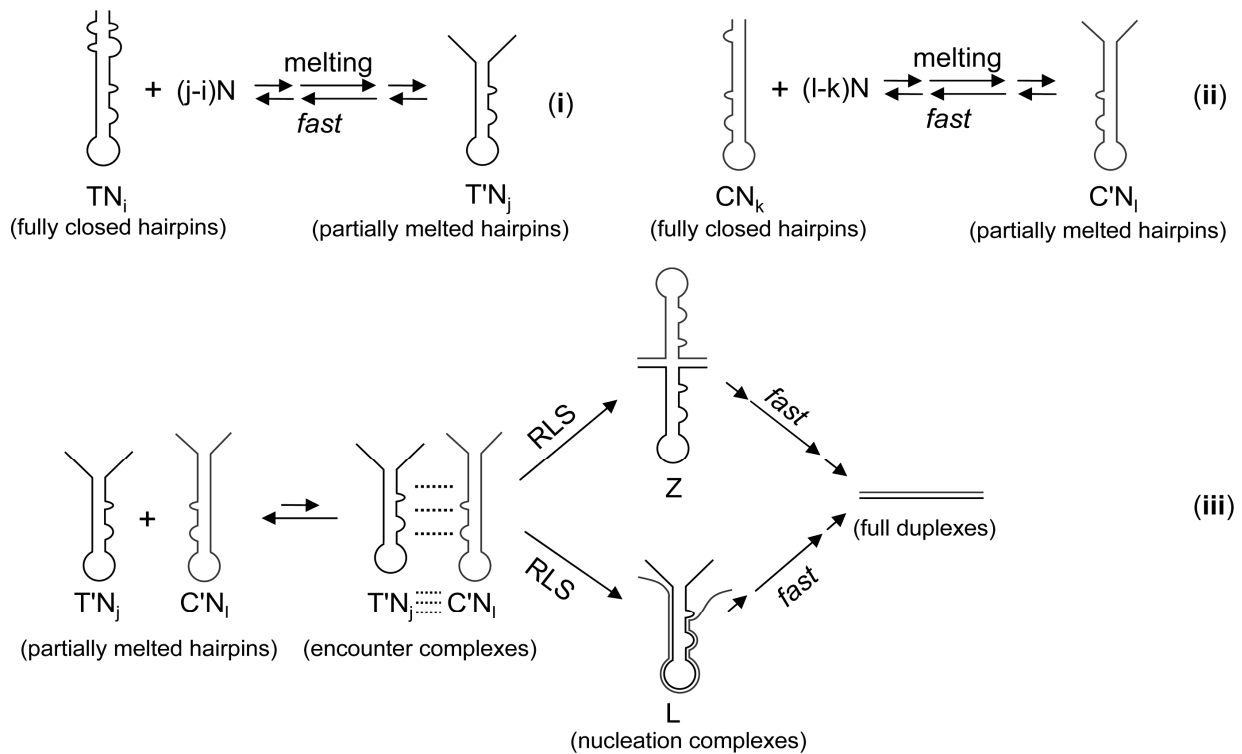
  

**Table S2.** Primary sequences of RRE IIB-related oligonucleotides and schematics illustrating the annealing reactions.

Oligonucleotides	Primary sequences
IIB RNA	5'-Cy3-UUUGGAGGUUAUAUGGGCGCAGCG CAAGCUGACGGUACAGGCCUCC(biotin)-3'
cIIB-1 DNA	5'- CCTGTACCGTCAGCTTGCGCTGCGCC CATATATTT-Cy5 -3'
cIIB-2 DNA	5'- TTGCGCTGCGCCCATATATTT-Cy5 -3'
Half-IIB RNA	5'-Cy3-UUAAAUAUAUGGGCGCAGCGC AA(biotin) -3'

**Table S3.** Summary of the chaperone and inhibition assays for HIV-1 RNA binding proteins or peptides

<b>Annealing reaction</b>	<b>NC chaperone activity</b>	<b>Inhibitor of NC induced annealing</b>	<b>These proteins have no chaperone activity</b>	<b>Specific binding</b>
TAR DNA + TAR RNA	Yes	Tat	<b>Tat &amp; Rev</b>	Tat binding to TAR RNA
TAR DNA + cTAR DNA	Yes	None	Tat & Rev	None
IIB + cIIB-1 DNA	Yes	Rev	<b>Rev &amp; Tat</b>	Rev binding to IIB RNA
IIB + cIIB-2 DNA	Yes	Rev	<b>Rev &amp; Tat</b>	Rev binding to IIB RNA
Half-IIB RNA + cIIB-2 DNA	Not required	-----	-----	None



**Scheme S1.** The hypothetical kinetic scheme of TAR DNA annealing to its complement chaperoned by HIV-1 NC. Here, T denotes TAR DNA, and C denotes complementary cTAR DNA or TAR RNA. The term N denotes the NC protein. In this scheme, N bound to T and C leads to a partially melted structure, namely the “Y” form of T (T’) and C(C’). The subscripts, i, j, k and l are used to describe the number of NCs bound to nucleotides. Two partially melted hairpins form an encounter complex that leads to the formation of nucleation complexes. The annealing can go through either zipper nucleation or loop nucleation, thereby forming zipper nucleation complexes (Z) or loop nucleation complexes (L) that lead to the formation of fully annealed duplexes. RLS stands for Rate Limiting Step.

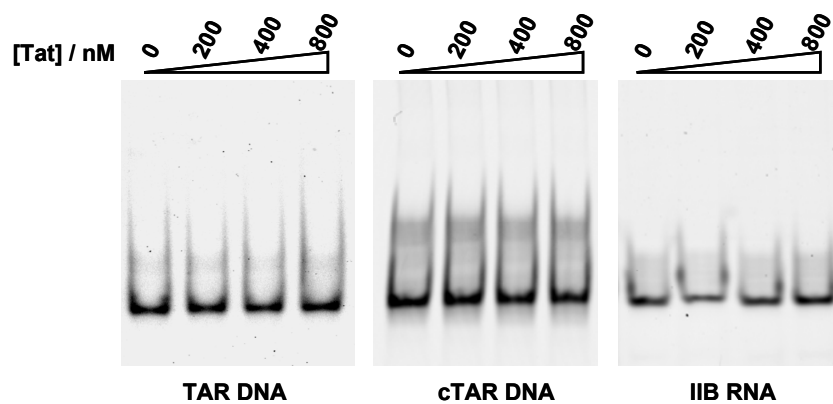


**Fig. S1.** Electrophoresis gel-shift assay of Tat binding to (*left*) TAR DNA, (*middle*) cTAR DNA, and (*right*) RRE-IIB RNA.

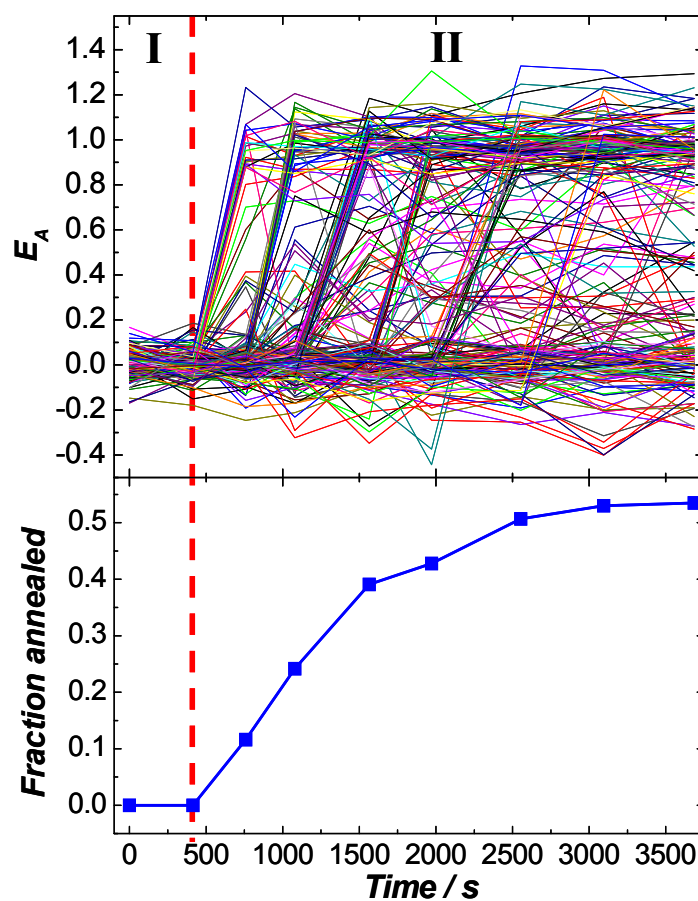


**Fig. S2.** SM-FRET trajectories of 215 molecules found in a  $30 \mu\text{m} \times 30 \mu\text{m}$  region (*upper panel*) and the fraction of annealed TAR DNA hairpins as a function of reaction time (*lower panel*) during the annealing of Cy5-labeled TAR RNA to immobilized Cy3-labeled TAR DNA. During time period I, 5 nM TAR RNA was flowed into the reaction chamber. During time period II, 5 nM TAR RNA and 800 nM NC were co-flowed into the reaction chamber.

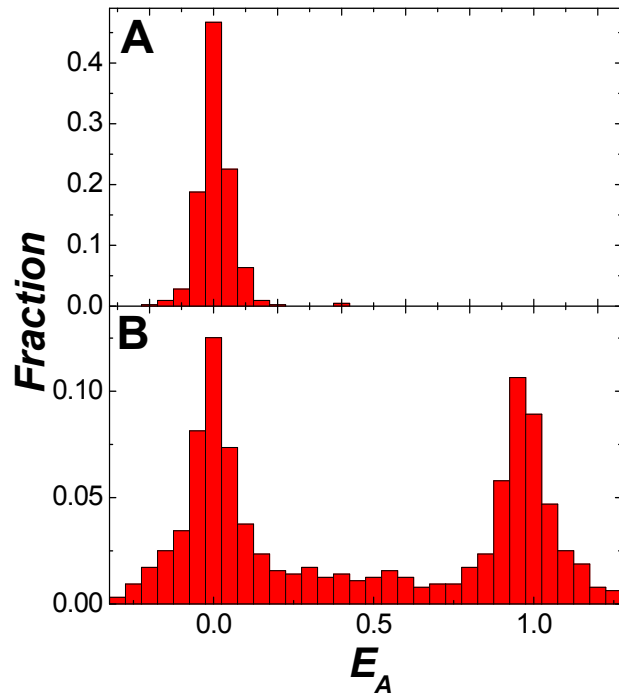


**Fig. S3.** FRET histograms obtained from SM-FRET measurements of (A) immobilized Cy3-TAR DNA in buffer and (B) after flowing in 5 nM Cy5-TRA RNA over immobilized Cy3-TAR DNA for 1 h in the presence of 800 nM NC and 800 nM Rev.

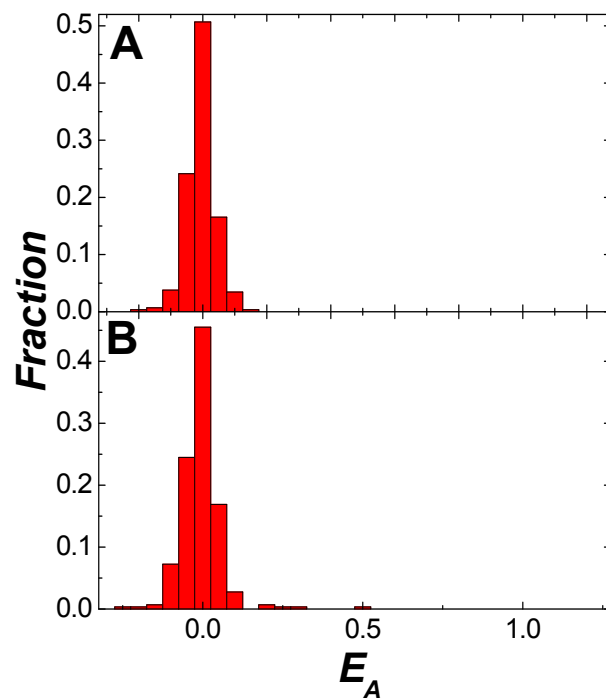


**Fig. S4.** FRET histograms obtained from SM-FRET measurements of (A) immobilized IIB RNA in buffer and (B) after flowing in 30 nM cIIB-1 DNA over immobilized IIB RNA for 2 h in the presence of 800 nM NC and 0.5 mM EDTA.

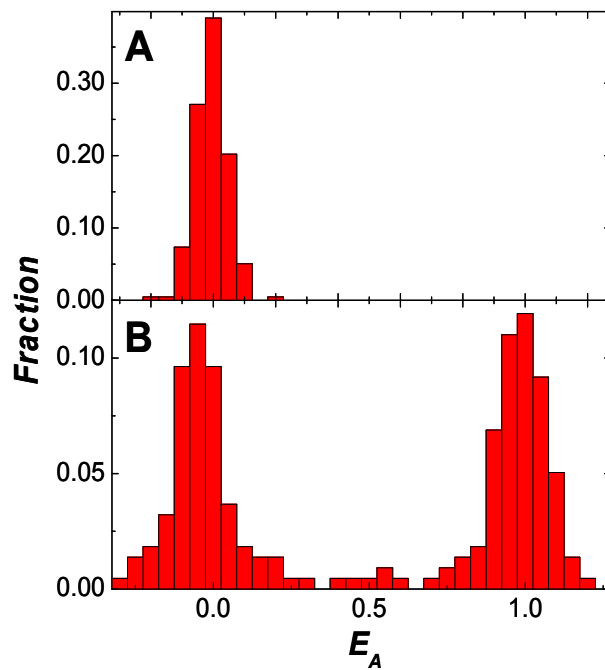


**Fig. S5.** FRET histograms obtained from SM-FRET measurements of (A) immobilized Half-IIB RNA in buffer and (B) after flowing in 30 nM cIIB-2 DNA over immobilized Half-IIB RNA for 2 h in the absence of any protein.